Eur. Phys. J. D (2015) 69: 191
DOI: 10.1140/epjd/e2015-60198-0

THE EUROPEAN PHYSICAL JOURNAL D

Regular Article

Non-classical effects in cavity QED containing a nonlinear optical medium and a quantum well: Entanglement and non-Gaussanity

A.-B. Mohamed[1,2,a] and H. Eleuch[3,4]

[1] College of Science, Prince Sattam Bin Abdulaziz University, Al-Aflaj, Saudi Arabia
[2] Faculty of Science, Assiut University, 71516 Assiut, Republic of Egypt
[3] Department of Physics, McGill University, Montreal, Canada H3A 2T8
[4] Department of Physics, Université de Montréal, Montreal, QC, H3T 1J4, Canada

Received 27 March 2015 / Received in final form 14 May 2015
Published online 4 August 2015 –

Abstract. Entanglement and non-Gaussianity are investigated in cavity QED containing a high optical nonlinear medium and a quantum well. It is shown that the dynamical behavior of the entanglement and the non-classicality are very sensitive to the initial state and the optical nonlinearities. By filling the cavity with the optical nonlinear medium, the non-Gaussianity as well as the light-matter entanglement is enhanced. For certain parameter sets, it is possible to control the degree and the dynamics of these quantum effects.

1 Introduction

Research into the nanosystems with exceptional proprieties is now a flourishing field in science and engineering. Thanks to their extremely small dimensions, they present an opportunity for new concepts and new applications such as biosensor, oriented medications, genetic manipulations [1–4] and quantum information [5,6].

Quantum correlation and more specifically the entanglement is the key concept for the quantum computation, quantum processing and quantum information [7–11]. In real quantum systems, quantum correlations are inevitably effected by the environment. Where the decoherence effects due to surrounding environment lead generally to the annihilation of these correlations [12–15]. This is a challenging problem for practical implementation of qubits and quantum gates in quantum information processing system. Hence, it is required to circumvent or reduce the environmental effects on quantum systems. To preserve the quantum correlation against decoherence, several approaches were proposed in reference [16–20].

It has been shown that cavity QED, including atomic or semiconductor systems, interacting with the environment exalt nonlinear and quantum effects [21–26] such as chaos [27], antibunching [28], squeezing [29] and entanglement [30,31]. Many typical quantum protocols depend crucially on the entanglement between the considered system, such as quantum cryptography [32,33], teleportation [34,35], and quantum computation [36]. A generation of entanglement is required. Recently, entanglement in semiconductor cavity QED is generated for particular initial states [37]. However the considered system contains only the excitonic nonlinearity. In our present work we explore the non-classical effects of a high nonlinear optical medium inside a cavity QED containing a quantum well.

The quantum phase-space concept has a wide popularity in several fields of physics [38,39]. There are different quantum phase-space distribution functions such as the Wigner function [40], Husimi function [41], and P function [42].

These functions are equivalent to one another, i.e., any of them can be used for the evaluation of the expectation value of any arbitrary operator. But Wigner function stands out among all distribution functions in quantum mechanics due to its real and non-singular proprieties. It gives correct expectation values of the operators in phase space. So, the positive and negative regions of WF are recently studied in different work [43–47].

In this work we analyze the entanglement dynamics and the time evolution of the WF in a cavity with a quantum well and a high nonlinear medium inside.

2 Model

The considered system is a good finesse cavity containing a nonlinear medium with the $(2q-1)$th optical nonlinearity and a semiconductor quantum well (The schematic of this system is presented in Fig. 1). The system is pumped by a coherent light creating a long lived photons inside the cavity. The intracavity electromagnetic wave interacts with the quantum well. A photon can excite an electron, in the quantum well, from the filled valence band to the

[a] e-mail: abdelbastm@yahoo.com

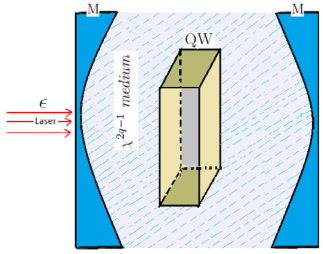

Fig. 1. Schematic model for a cavity containing a quantum well (QW) and a high nonlinear optical medium.

conduction band creating a hole in the valence band. The interaction between the excited electron and the hole creates an exciton. The exciton is then coupled coherently to an intracavity photon. In order to maximize the photon-exciton coupling, the quantum well (QW) is placed in the middle of the cavity where the intracavity electromagnetic field is at its maximum. For cavity QED systems, it is known that the nonlinearity is responsible for the appearance of nonclassical effects such as squeezing and entanglement [29–31]. In our system, the cavity is filled with a high nonlinear optical medium in contemplation of increasing the nonclassical effects and in particular the entanglement.

The Hamiltonian of the considered system is given by:

$$H = H_{nl} + H_c + H_{ex} + H_p, \tag{1}$$

where H_{nl} represents the Hamiltonian of the $(2q-1)$th nonlinear media [48]

$$H_{nl} = \hbar\chi^{(2q-1)}(\hat{a}^\dagger)^q\hat{a}^q, \tag{2}$$

$\hat{a}$ and $\hat{a}^\dagger$ represent the creation and annihilation operators of the optical mode. $\chi^{(2q-1)}$ is the nonlinear optical susceptibility of the nonlinear medium. H_{ex} designs the Hamiltonian of the exciton [49–51]

$$H_{ex} = \hbar\omega_{ex}\hat{b}^\dagger\hat{b} + \hbar\alpha'\hat{b}^\dagger\hat{b}^\dagger\hat{b}\hat{b}, \tag{3}$$

where $\hat{b}$ and $\hat{b}^\dagger$ are the excitonic annihilation and creation operators. The second term describes the interaction between neighbor excitons inside the quantum. α' and ω_{ex} are respectively the non-linearity and the frequency of the exciton. The Hamiltonian of the exciton-photon interaction is given by:

$$H_c = \hbar g'\left(\hat{a}^+\hat{b} + \hat{b}^+\hat{a}\right). \tag{4}$$

The system is pumped by a coherent laser light. The Hamiltonian corresponding to the pump is given by:

$$H_p = \hbar\epsilon'\left(\hat{a}^+e^{i\omega_L t} + \hat{a}e^{-i\omega_L t}\right), \tag{5}$$

where ω_L and ϵ' design the frequency and the amplitude of the pump laser. We restrict our analysis to the case of the resonance ($\omega_{ex} = \omega_L$). In the interaction representation the Hamiltonian becomes

$$H_{int} = \hbar\chi^{(2q-1)}\left(\hat{a}^\dagger\right)^q\hat{a}^q + \hbar g'\left(\hat{a}^+\hat{b} + \hat{b}^+\hat{a}\right) + \hbar\alpha' b^\dagger b^\dagger\hat{b}\hat{b} + \hbar\epsilon'\left(\hat{a}^+ + \hat{a}\right). \tag{6}$$

Further more, we neglect the nonlinear dissipations [23] and we suppose that the thermal reservoir temperature $T = 0$, then we can write [52–54]

$$\frac{\partial\rho}{\partial t} = i\hbar[H_{int},\rho] + \kappa\left(2\hat{a}\rho\hat{a} - \hat{a}^\dagger\hat{a}\rho - \rho\hat{a}^\dagger\hat{a}\right) + \frac{\gamma}{2}\left(2\hat{b}\rho\hat{b} - \hat{b}^\dagger\hat{b}\rho - \rho\hat{b}^\dagger\hat{b}\right). \tag{7}$$

t represents a unitless time normalized to τ_c, where τ_c is the round trip time for a photon inside the cavity. We normalize also the parameters of the system to $1/\tau_c$ as: $g = g\tau_c$, $\alpha = \alpha'\tau_c$, $\epsilon = \epsilon'\tau_c$. $\frac{\gamma}{2}$ and κ represent respectively the normalized excitonic spontaneous emission and the cavity dissipation rates.

For the weak pumping regime $\frac{\epsilon}{\kappa} \ll 1$, $2\hat{a}\rho\hat{a}$ and $2\hat{b}\rho\hat{b}$ can be neglected in (3) [49,51]. Thus we obtain [51,55,56]

$$i\frac{d}{dt}\rho = \hat{H}_{eff}\rho - (\rho\hat{H}_{eff})^\dagger, \tag{8}$$

where H_{eff} is defined as the effective non-Hermitian Hamiltonian

$$H_{eff} = \chi^{(2q-1)}\left(a^\dagger\right)^q\hat{a}^q + g\left(\hat{a}^+\hat{b} + \hat{b}^+\hat{a}\right) + \hbar\alpha\hat{b}^\dagger\hat{b}^\dagger\hat{b}\hat{b} + \epsilon\left(\hat{a}^+ + \hat{a}\right) - i\kappa\hat{a}^\dagger\hat{a} - i\frac{\gamma}{2}\hat{b}^\dagger\hat{b}. \tag{9}$$

Equation (8) can be reduced to

$$\frac{d}{dt}|\psi(t)\rangle = -i\,\hat{H}_{eff}|\psi(t)\rangle, \tag{10}$$

where

$$|\psi(t)\rangle = \sum A_{ij}|ij\rangle. \tag{11}$$

$|ij\rangle = |i\rangle\otimes|j\rangle$, i and j represent the numbers of photons and excitons inside the cavity.

Let us define the number of excitations N for each state $|ij\rangle$ as $N = i + j$, the number of excitons added to the number of photons inside the cavity.

For the weak pumping regime, the maximum number of excitations can be limited to $N_{max} = 6$, we then get

$$|\psi(t)\rangle = \sum_{i+j\leq 6} A_{ij}|ij\rangle. \tag{12}$$

It is worth to note that in order to explore the dynamics of this system, we need in general $\sum_{k=1}^{N_{\max}+1} k = [\frac{(N_{\max}+1)(N_{\max}+2)}{2}]$ differential equations for the amplitudes A_{ij} (examples of the differential equations of A_{ij} in similar systems are presented in Refs. [37,55,56]).

The amplitudes $A_{ij}(t)$ verify the following differential equations (derived from the non-Hermitian Shrödinger equation):

$$
\begin{aligned}
\dot{A}_{00} &= -\mu_{00}A_{00} - i\epsilon A_{10},\\
\dot{A}_{01} &= -\mu_{01}A_{01} - igA_{10} - i\epsilon A_{11},\\
\dot{A}_{02} &= -\mu_{02}A_{02} - ig\sqrt{2}A_{11} - i\epsilon A_{12},\\
\dot{A}_{03} &= -\mu_{03}A_{03} - ig\sqrt{3}A_{12} - i\epsilon A_{13},\\
\dot{A}_{04} &= -\mu_{04}A_{04} - i2gA_{13} - i\epsilon A_{14}\\
\dot{A}_{05} &= -\mu_{05}A_{05} - ig\sqrt{5}A_{14} - i\epsilon A_{15},\\
\dot{A}_{06} &= -\mu_{06}A_{06} - ig\sqrt{6}A_{15},\\
\dot{A}_{10} &= -\mu_{10}A_{10} - ig\eta_{10} - i\epsilon(A_{00} + \sqrt{2}A_{20}),\\
\dot{A}_{11} &= -\mu_{11}A_{11} - ig\eta_{11} - i\epsilon(A_{01} + \sqrt{2}A_{21}),\\
\dot{A}_{12} &= -\mu_{12}A_{12} - ig\eta_{12} - i\epsilon(A_{02} + \sqrt{2}A_{22}),\\
\dot{A}_{13} &= -\mu_{13}A_{13} - ig\eta_{13} - i\epsilon(A_{03} + \sqrt{2}A_{23}),\\
\dot{A}_{14} &= -\mu_{14}A_{14} - ig\eta_{14} - i\epsilon(A_{04} + \sqrt{2}A_{24}),\\
\dot{A}_{15} &= -\mu_{15}A_{15} - ig\eta_{15} - i\epsilon A_{05},\\
\dot{A}_{20} &= -\mu_{20}A_{20} - ig\eta_{20} - i\epsilon(\sqrt{2}A_{10} + \sqrt{3}A_{30}),\\
\dot{A}_{21} &= -\mu_{21}A_{21} - ig\eta_{21} - i\epsilon(\sqrt{2}A_{11} + \sqrt{3}A_{31}),\\
\dot{A}_{22} &= -\mu_{22}A_{22} - ig\eta_{22} - i\epsilon(\sqrt{2}A_{12} + \sqrt{3}A_{32}),\\
\dot{A}_{23} &= -\mu_{23}A_{23} - ig\eta_{23} - i\epsilon(\sqrt{2}A_{13} + \sqrt{3}A_{33}),\\
\dot{A}_{24} &= -\mu_{24}A_{24} - ig\eta_{24} - i\epsilon\sqrt{2}A_{14},\\
\dot{A}_{30} &= -\mu_{30}A_{30} - ig\eta_{30} - i\epsilon(\sqrt{3}A_{20} + \sqrt{4}A_{40}),\\
\dot{A}_{31} &= -\mu_{31}A_{31} - ig\eta_{31} - i\epsilon(\sqrt{3}A_{21} + \sqrt{4}A_{41}),\\
\dot{A}_{32} &= -\mu_{32}A_{32} - ig\eta_{32} - i\epsilon(\sqrt{3}A_{22} + \sqrt{4}A_{42}),\\
\dot{A}_{33} &= -\mu_{33}A_{33} - ig\eta_{33} - i\epsilon\sqrt{3}A_{23},\\
\dot{A}_{40} &= -\mu_{40}A_{40} - ig\eta_{40} - i\epsilon(\sqrt{4}A_{30} + \sqrt{5}A_{50}),\\
\dot{A}_{41} &= -\mu_{41}A_{41} - ig\eta_{41} - i\epsilon(\sqrt{4}A_{31} + \sqrt{5}A_{51}),\\
\dot{A}_{42} &= -\mu_{42}A_{42} - ig\eta_{42} - i\epsilon\sqrt{4}A_{32},\\
\dot{A}_{50} &= -\mu_{50}A_{40} - ig\eta_{50} - i\epsilon(\sqrt{5}A_{40} + \sqrt{6}A_{60}),\\
\dot{A}_{51} &= -\mu_{51}A_{51} - ig\eta_{51} - i\epsilon\sqrt{5}A_{41},\\
\dot{A}_{60} &= -\mu_{60}A_{60} - ig\eta_{60} - i\epsilon\sqrt{6}A_{50}. \qquad (13)
\end{aligned}
$$

Here $\mu_{mn} = m\kappa + \frac{n}{2}\gamma + i(m^2 - m)\alpha + i\beta_m$, $\eta_{mn} = \sqrt{m(n+1)}A_{(m-1)(n+1)} + \sqrt{(m+1)n}A_{(m+1)(n-1)})$ and $\beta_n = \frac{n!\chi^{(2q-1)}}{(n-q)!}$. In order to compute the wave function $|\psi(t)\rangle$, we should solve the system of differential equations above. For the density matrix (of state (12)) given by $\rho_{ce}(t) = |\psi(t)\rangle\langle\psi(t)|$, the reduced system density matrix of the cavity (exciton) can be written as

$$\rho_{c(e)}(t) = \mathrm{Tr}_{e(c)}\{|\psi(t)\rangle|\psi(t)|\} = \sum_{m,n}\rho^{c(e)}_{m,n}(t). \qquad (14)$$

The reduced density matrices allow us to determine any property related to the excitonic or the optical modes. In the next section we explore the dynamics of the entanglement and the Wigner function.

3 Entanglement and Wigner function

3.1 Entanglement via von Neumann entropy

Methods of quantifying entanglement have only been found in the last decades [57]. For pure bipartite quantum states several physically measures of entanglement have been established (see for example [58,59]), while for general mixed state of n-partite systems, the measure of entanglement still under development. As a measure of entanglement between the photons and excitons, we use the reduced quantum entropy. More precisely, we adopt the von Neumann entropy to measure the entanglement of the generated state. It is defined as [60]: $S(\rho) = -\mathrm{Tr}\rho\ln\rho$. For the reduced density matrix $\rho_c = \mathrm{Tr}_e\{|\psi(t)\rangle|\psi(t)|\}$, the reduced entropy of the resulted state ρ_c is

$$S_c = -\sum_i \lambda_i \ln\lambda_i, \qquad (15)$$

where λ_i are the eigenvalues of the reduced density matrix ρ_c of the optical mode. The entropy of a general two-components quantum system are linked by the theorem of Araki and Lieb [61]: $|S_c - S_e| \leq S_{ce} \leq S_c + S_e$, where S_{ce} is the total entropy of the photons-exciton system. We note that the S_{ce} depends on ρ_{ce} which has an unitary time evolution, and consequently the total entropy S_{ce} is time independent. Since we assume that the photons and excitons are initially in a disentangled pure state, the total entropy vanishes.

One immediate consequence of this assumption is $S_c = S_e$. Consequently, we only need to calculate one of them, say S_c, to discuss the photon-exciton entanglement. If a bipartite system is in a pure state and composed of subsystems A and B (with the density matrix ρ^{AB}), where each subsystem of them has $(n+1)$-states, $\{|0\rangle, |1\rangle, ..., |n\rangle\}$, the maximum value of the sub-entropy is given by: $0 \leq S_i \leq S_i^{max} = \ln(n+1), (i = A, B)$ [62].

For example, if the subsystems A and B are (qubits), $\{|0\rangle, |1\rangle\}$, then the value of the maximum entropy is $S_i^{max} = \ln 2 \approx 0.7$.

In our work, the allowed states for the optical mode as well as for the exciton are: $\{|0\rangle, |1\rangle, \ldots, |6\rangle\}$ which give $S_i^{max} = \ln 7 = 1.9459$. We note that the maximum value of the entropy used to measure the level of entanglement, differs from the maximum value of the other entanglement measures such as the concurrence and the negativity.

We numerically compute the solutions of the system of the differential equations (13) in order to study the entanglement between the excitonic and the optical modes. The von Neumann entropy for the initial state $|\psi(0)\rangle = \frac{1}{\sqrt{3}}(|11\rangle + |22\rangle + |33\rangle)$ with different values of (κ, γ) is shown in Figure 2 for fixed values $(g, q, \epsilon, \chi, \alpha) = (1, 3, 10^{-3}, 10^{-3}, 10^{-9})$. For weak dissipation rates $(\kappa, \gamma) = (0.01, 0)$, von Neumann entropy oscillates periodically with time. Therefore, the entanglement is generated and lost via the interaction between the excitonic and optical modes. For different values of the dissipation rates (κ, γ), von Neumann entropy decays exponentially to zero. The finishing of von Neumann entropy

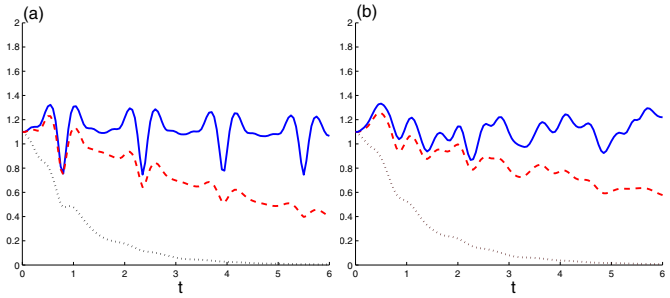

Fig. 2. Von Neumann entropy for the initial state $|\psi(0)\rangle = \frac{1}{\sqrt{3}}(|11\rangle + |22\rangle + |33\rangle)$ with $(\kappa, \gamma) = (0.01, 0)$ (solid curve), $(\kappa, \gamma) = (0.1, 0)$ (dashed curve) and $(\kappa, \gamma) = (0.3, 0.4)$ (dot curve). The normalized values of the parameters are: $(g, q, \epsilon, \alpha) = (1, 3, 10^{-3}, 10^{-9})$, $\chi = 10^{-3}$ for (a) and $\chi = 0.9$ for (b).

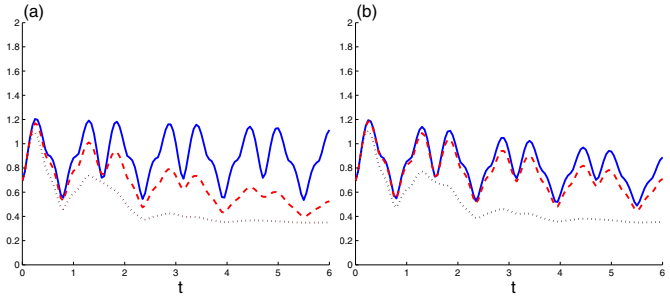

Fig. 3. Von Neumann entropy for $|\psi(0)\rangle = \frac{1}{\sqrt{2}}(|00\rangle + |22\rangle)$ with different values of $\kappa = 0.01$ (solid curve), 0.1 (dashed curve), 0.3 (dot curve) in (a) and for different values of γ in (b) $\gamma = 0.05$ (solid curve), 0.1 (dashed curve) and 0.5 (dot curve). The normalized values of the parameters are: $(g, q, \chi, \epsilon, \alpha) = (1, 3, 10^{-3}, 10^{-3}10^{-9})$, $\gamma = 0$ for (a) and $\kappa = 0.01$ for (b).

depends on excitonic spontaneous emission and cavity dissipation rates. The effect of the high optical nonlinearity $(\chi, q) = (0.9, 3)$ is shown in Figure 2b, where the regularity of von Neumann entropy disappears.

For the initial states $|\psi(0)\rangle = \frac{1}{\sqrt{2}}(|00\rangle + |22\rangle)$ and $|\psi(0)\rangle = \frac{1}{\sqrt{2}}(|00\rangle + |33\rangle)$, the effect of the excitonic spontaneous emission and cavity dissipation rates are shown in Figures 3 and 4 respectively with the parameters values $(g, q, \chi, \epsilon, \alpha) = (1, 3, 10^{-3}, 10^{-3}, 10^{-9})$. These initial states generate entanglement more than that is generated by the initial state $|\psi(0)\rangle = \frac{1}{\sqrt{3}}(|11\rangle + |22\rangle + |33\rangle)$. With the increase of the dissipation rates κ and γ, von Neumann entropy decays exponentially to its stationary entanglement (non-zero values for von Neumann entropy). The stationary entanglement values do not dependent on the excitonic spontaneous emission and cavity dissipation rates. However the entanglement attains its stationary state earlier in time for higher dissipation rates.

From Figures 5 and 6, we can conclude that the entanglement is reduced for some initial states and enhanced for others. This effect can be seen for the following entangled pure states: $\frac{1}{\sqrt{2}}(|00\rangle + |11\rangle)$, $\frac{1}{\sqrt{3}}(|00\rangle + |11\rangle + |22\rangle)$ and $\frac{1}{\sqrt{4}}(|00\rangle + |11\rangle + |22\rangle + |33\rangle)$. These initial states have

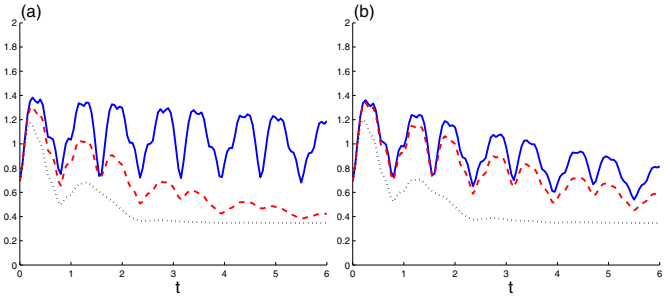

Fig. 4. Von Neumann entropy for $|\psi(0)\rangle = \frac{1}{\sqrt{2}}(|00\rangle + |33\rangle)$ with $\kappa = 0.01$ (solid curve), 0.1 (dashed curve), 0.3 (dot curve) and for different values of γ in (b) $\gamma = 0.05$ (solid curve), 0.1 (dashed curve) and 0.5 (dot curve). The normalized values of the parameters are: $(g, q, \chi, \epsilon, \alpha) = (1, 3, 10^{-3}, 10^{-3}10^{-9})$, $\gamma = 0$ for (a) and $\kappa = 0.01$ for (b).

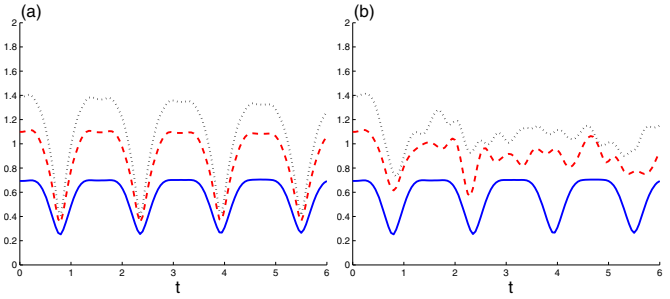

Fig. 5. Von Neumann entropy for the initial state $\frac{1}{\sqrt{2}}(|00\rangle + |11\rangle)$ (solid curve), $\frac{1}{\sqrt{3}}(|00\rangle + |11\rangle + |22\rangle)$ (dashed curve) and $\frac{1}{\sqrt{4}}(|00\rangle + |11\rangle + |22\rangle + |33\rangle)$ (dot curve). The normalized values of the parameters are: $(g, q, \gamma, \kappa, \epsilon, \alpha) = (1, 3, 0, 10^{-2}, 10^{-3}, 10^{-9})$, $\chi = 10^{-3}$ for (a) and $\chi = 0.9$ for (b).

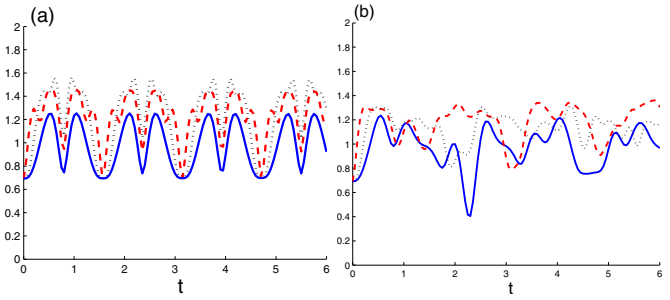

Fig. 6. Von Neumann entropy for the initial state $\frac{1}{\sqrt{2}}(|11\rangle + |22\rangle)$ (solid curve), $\frac{1}{\sqrt{2}}(|11\rangle + |33\rangle)$ (dashed curve) and $\frac{1}{\sqrt{2}}(|22\rangle + |33\rangle)$ (dot curve). The normalized values of the parameters are: $(g, q, \gamma, \kappa, \epsilon, \alpha) = (1, 3, 0, 10^{-2}, 10^{-3}, 10^{-9})$, $\chi = 10^{-3}$ for (a) and $\chi = 0.9$ for (b).

periodic oscillations of their entanglement see Figures 5a and 6a. This regularity of the entanglement dynamics disappears for high nonlinear optical media $(\chi, q) = (0.9, 3)$ (see Figs. 5b and 6b).

The effect of the $3rd$ order optical nonlinearity $(2q - 1 = 3)$ is shown in Figures 7 and 8. By comparing the effect for 3rd and 5th order nonlinearities (see Figs. 2, 3, 7 and 8) on the dynamical behavior of the entanglement,

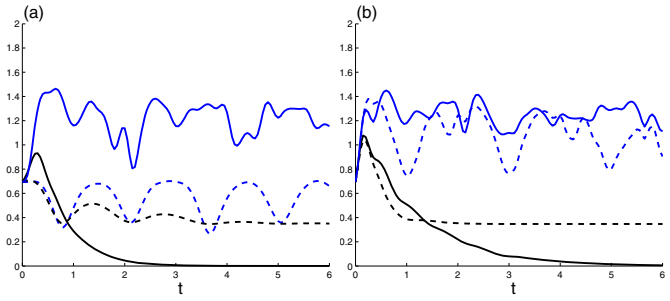

Fig. 7. Von Neumann entropy for the initial state $\frac{1}{\sqrt{2}}(|00\rangle + |11\rangle)$ (dashed curve) and $\frac{1}{\sqrt{2}}(|22\rangle + |33\rangle)$ (solid curve) with $(\gamma, \kappa, \epsilon) = (0, 10^{-2}, 10^{-3})$ in two upper curves and $(\gamma, \kappa, \epsilon) = (0.5, 0.3, 0.03)$ in lower upper curves in (a) and for $\frac{1}{\sqrt{2}}(|00\rangle + |33\rangle)$ (dashed curve) and $\frac{1}{\sqrt{2}}(|11\rangle + |33\rangle)$ (solid curve) in (b). The normalized values of the parameters are $(g, \chi, q, \alpha) = (1, 0.9, 2, 10^{-9})$.

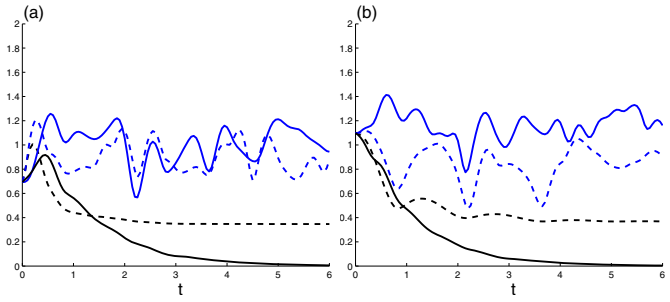

Fig. 8. As Figure 7 but for $\frac{1}{\sqrt{2}}(|00\rangle + |22\rangle)$ (dashed curve) and $\frac{1}{\sqrt{2}}(|11\rangle + |22\rangle)$ (solid curve) in (a) and for $\frac{1}{\sqrt{3}}(|00\rangle + |11\rangle + |22\rangle)$ (dashed curve) and $\frac{1}{\sqrt{3}}(|11\rangle + |22\rangle + |33\rangle)$ (solid curve) in (b).

we observe a notable changes. We can deduce that the entanglement dynamics is very sensitive not only to the initial states as mentioned before but also to the order of the optical nonlinearity.

3.2 Wigner function

The Wigner function (WF) is a powerful tool to study the non-classicality of optical fields. The partial negativity of WF implies non-classical proprieties of the quantum states. The WF presents several advantages compared to the other quasi-probability distributions in quantum mechanics [41]. Namely, it is non-singular and real. It yields to correct quantum mechanical operator averages in phase space and posses defined marginal distributions. Furthermore, the phase space concept of the Wigner function describes the dynamics of quantum systems.

The Wigner function for any system with density matrix ρ is defined in terms of coherent state parameters α and β as [63,64]

$$W(\alpha, t) = \frac{1}{\pi^2} \int Tr[\hat{\rho} e^{\beta \hat{a}^+ - \beta^* \hat{a}}] e^{\alpha \beta^* - \alpha^* \beta} d^2\beta, \qquad (16)$$

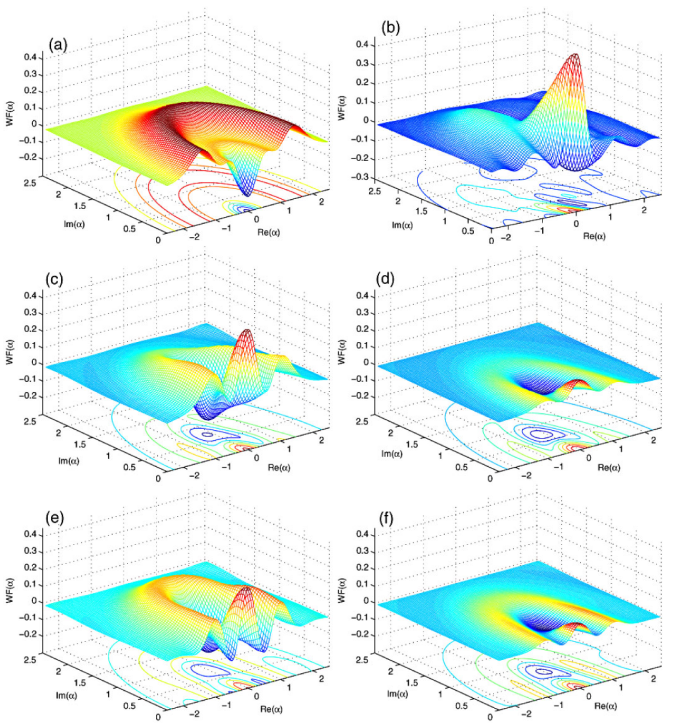

Fig. 9. Wigner function for the optical mode for the initial state $\frac{1}{\sqrt{3}}(|11\rangle + |22\rangle + |33\rangle)$ in (a). WF at $t_{\max} = 2.3$ for different values of $(\kappa, \gamma, \chi, q)$: $(0.01, 0, 10^{-3}, 3)$ in (b), $(0.01, 0, 0.9, 3)$ in (c) and $(0.1, 0.2, 0.9, 3)$ in (d). (e, f) as (c, d) with $q = 2$. The other normalized values are $(g, \epsilon, \alpha) = (1, 0.001, 10^{-9})$.

where β is the amplitude of the coherent state $|\beta\rangle = \hat{D}(\beta)|0\rangle$ and $\hat{D}(\beta) = \exp(\beta \hat{a}^+ - \beta^* \hat{a})$ is the displacement operator. Wigner function is experimentally measured for a field stored inside a high-Q cavity [65,66]. The expression of the Wigner function for the optical mode is [43–45],

$$W(\alpha, t) = \frac{2}{\pi} \sum_{p=0}^{\infty} \sum_{n,m=0}^{\infty} (-1)^p \rho^c_{m,n}(t) \langle \alpha, p|n\rangle \langle m|\alpha, p\rangle,$$

where

$$\langle m|\alpha, p\rangle = e^{\frac{-|\alpha|^2}{2}} \sum_{j=0}^{min(p,m)} \frac{(-\alpha^*)^{(p-j)} (\alpha)^{m-j} \sqrt{p!m!}}{(m-j)!(p-j)!j!}.$$

$\rho^c_{m,n}$ are the matrix elements of the reduced density matrix $\hat{\rho}_c(t)$ of the optical mode given by equation (13), α represents a complex number (the amplitude of the coherent state), in our work, we take the phase-space: $\mathrm{Re}(\alpha) \in [-\frac{8\pi}{10}, \frac{8\pi}{10}]$ and $\mathrm{Im}(\alpha) \in [0, \frac{8\pi}{10}]$. The range chosen intervals of the phase-space are due to the symmetries of the Wigner Function on $\mathrm{Re}(\alpha)$ and $\mathrm{Im}(\alpha)$. The second goal of this paper is to explore the effects of the nonlinear medium on the non-classicality of the optical mode by analyzing the Winger function behavior.

The non-classicality of the optical mode can be deduced from the nature of the Wigner function. In Figures 9–13, The Wigner function of the optical mode is

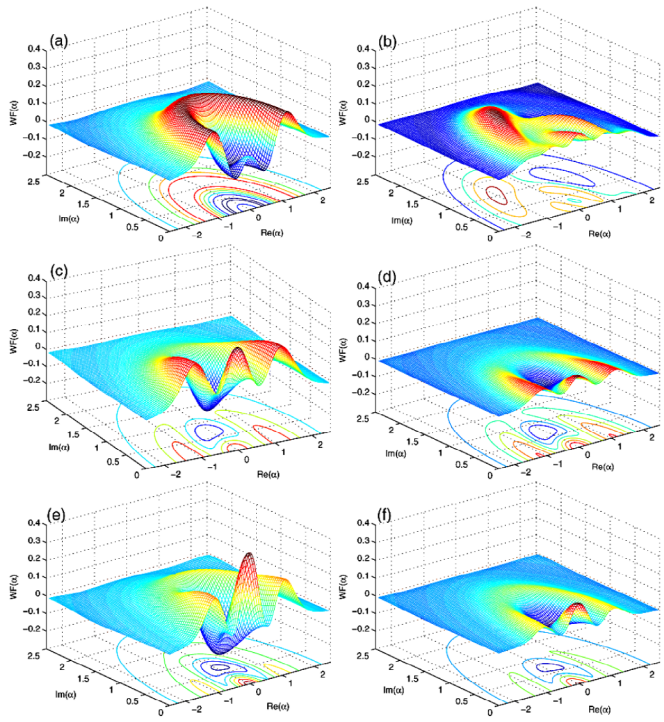

Fig. 10. Wigner function for the initial state $\frac{1}{\sqrt{2}}(|11\rangle + |22\rangle)$ in (a). WF at $t_{\max} = 2.1$ for different values of $(\kappa, \gamma, \chi, q)$: $(0.01, 0, 10^{-3}, 3)$ in (b), $(0.01, 0, 0.9, 3)$ in (c) and $(0.1, 0.2, 0.9, 3)$ in (d). (e, f) as (c, d) with $q = 2$. The other normalized values are: $(g, \epsilon, \alpha) = (1, 0.001, 10^{-9})$.

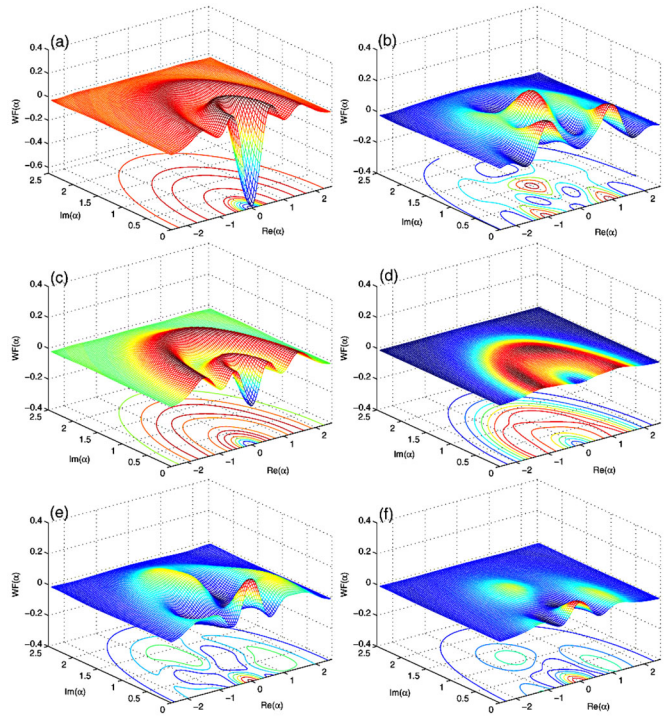

Fig. 11. Wigner function for the initial state $\frac{1}{\sqrt{2}}(|11\rangle + |33\rangle)$ in (a). WF at $t_{\max} = 2.0$ for different values of $(\kappa, \gamma, \chi, q)$: $(0.01, 0, 10^{-3}, 3)$ in (b), $(0.01, 0, 0.9, 3)$ in (c) and $(0.1, 0.2, 0.9, 3)$ in (d). (e, f) as (c, d) with $q = 2$. The other normalized values are: $(g, \epsilon, \alpha) = (1, 0.001, 10^{-9})$.

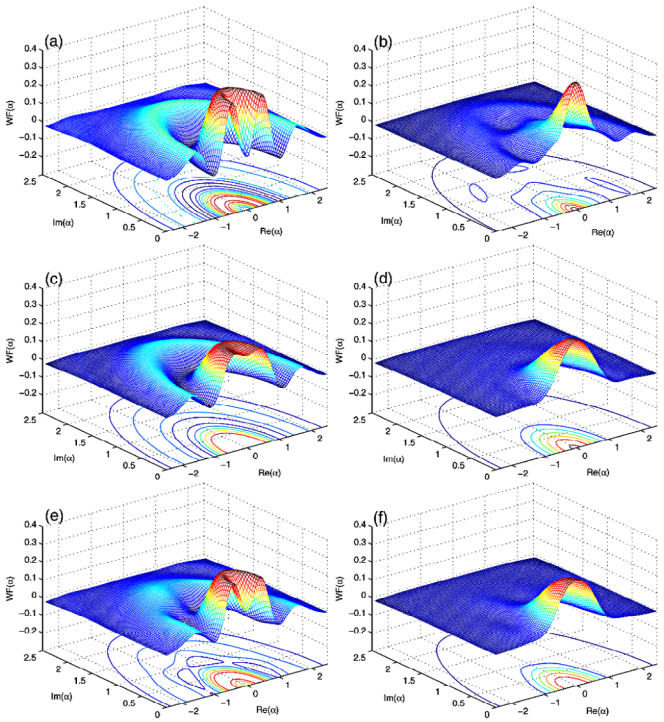

Fig. 12. Wigner function for the initial state $\frac{1}{\sqrt{2}}(|00\rangle + |33\rangle)$ in (a). WF at $t_{\max} = 1.8$ for different values of $(\kappa, \gamma, \chi, q)$: $(0.01, 0, 10^{-3}, 3)$ in (b), $(0.01, 0, 0.9, 3)$ in (c) and $(0.1, 0.2, 0.9, 3)$ in (d). (e, f) as (c, d) with $q = 2$. The other normalized values are: $(g, \epsilon, \alpha) = (1, 0.001, 10^{-9})$.

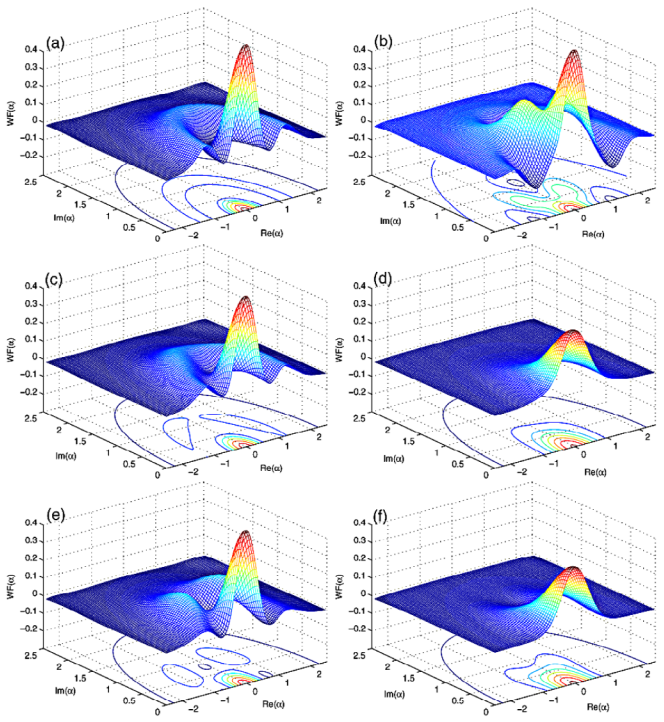

Fig. 13. Wigner function for the initial state $\frac{1}{\sqrt{2}}(|00\rangle + |22\rangle)$ in (a). WF at $t_{\max} = 2.35$ for different values of $(\kappa, \gamma, \chi, q)$: $(0.01, 0, 10^{-3}, 3)$ in (b), $(0.01, 0, 0.9, 3)$ in (c) and $(0.1, 0.2, 0.9, 3)$ in (d). (e, f) as (c, d) with $q = 2$. The other normalized values are: $(g, \epsilon, \alpha) = (1, 0.001, 10^{-9})$.

plotted for different initial entangled states. For each initial state, we investigate the following: (i) WF for the state of the optical mode at the times $t = 0$ and $t_{\max}$(at which the von Neumann entropy has a maximum value). (ii) the effects of the optical nonlinearity and the dissipation rates.

In Figure 9a, we plot the Wigner function for the initial state $\frac{1}{\sqrt{3}}(|11\rangle + |22\rangle + |33\rangle)$ (at $t = 0$). The other plots of Figure 9 represent the evolution of the Wigner function at $t_{\max} = 2.3$ where the Von Neumann entropy is maximum for different values of the optical nonlinearity parameters (χ and q). By increasing the optical nonlinearities (χ and q) more pronounced negative regions of the Wigner function appear. This effect clearly indicates an increasing of the non-classicality for the final states. For two different initial states (namely $\frac{1}{\sqrt{3}}(|11\rangle + |22\rangle + |33\rangle)$ for Fig. 10 and $\frac{1}{\sqrt{2}}(|11\rangle + |22\rangle)$ for Fig. 11), we observe similar behavior by increasing the nonlinear optical parameters. This confirms the fact that the increase of the optical nonlinearity enhances the non-classicality of the optical states. As expected, Figures 12 and 13 affirm that the dissipations destroy the non-classicality of the optical states. It is worth to note that the observed parameter effects on the non-classicality (Figs. 9–13) are similar to the dynamical entanglement (Figs. 2–8). More precisely, the optical nonlinearities increase the non-classicality and the entanglement, while the dissipations reduce or destroy these two effects.

4 Conclusion

In this work, the entanglement dynamics in a cavity QED filled with a nonlinear optical medium and containing a quantum well is investigated. The negativity of the Wigner function as a measure of the non-classicality is discussed. The dynamical entanglement measured by von Neumann entropy as well as the non-classicality is very sensitive to the initial state, the amplitude and the order of the optical nonlinearities. The optical nonlinearities amplify these non-classical effects, while depending on the initial state, they can be reduced or enhanced. Our analysis shows that by filling the cavity with a high optical nonlinear medium, the non-Gaussianity of the optical mode and the light-matter entanglement (exciton-photon entanglement) are enhanced. The control of these quantum effects is possible. For some sets of the system parameters it may be possible not only to optimize the entanglement and the non-Gaussianity but also to control their dynamics. Recent experimental progress on entanglement observation in similar systems [67–69] pave the way to the realization of this proposal. Furthermore, The non-Gaussianity control may open the door to the conception of optical states with unconventional proprieties. Our results may also lead to new applications in quantum engineering through an optimal design and control of the entanglement.

This project was supported by the deanship of scientific research at Prince Sattam bin Abdulaziz university under the research project No. 2014/01/2757. The authors contributed equally to the paper.

References

1. V.K. Varadan, L. Chen, J. Xie, *Nanomedicine: Design and Applications of Magnetic Nanomaterials, Nanosensors and Nanosystems* (Wiley, New York, 2008)
2. E. Kobayashi, A.K. Iyer, F.J. Hornicek, M.M. Amiji, Z. Duan, Clin. Orthop. Relat. Res. **471**, 915 (2013)
3. Ch. Tan, S. Saurabh, M.P. Bruchez, R. Schwartz, P. LeDuc, Nat. Nanotechnol. **8**, 602 (2013)
4. P. Sanjenbam, J.V. Gopal, K. Kannabiran, J. Med. Mycol. **24**, 211 (2014)
5. M.R. Henderson, B.C. Gibson, H. Ebendorff-Heidepriem, K. Kuan, V.S. Afshar, J.O. Orwa, I. Aharonovich, S. Tomljenovic-Hanic, A.D. Greentree, S. Prawer, T.M. Monro, Adv. Mater. **23**, 2806 (2011)
6. O.N. Gadomskii, Y.Y. Kharitonov, Quantum Electron. **34**, 249 (2011)
7. M.A. Nielsen, I.L. Chuang, *Quantum Computation and Quantum Information* (Cambridge University Press, Cambridge, 2000)
8. K. Berrada, H. Eleuch, Y. Hassouni, J. Phys. B **44**, 145503 (2011)
9. J.M. Raimond, M. Brune, S. Haroche, Rev. Mod. Phys. **73**, 565 (2001)
10. R. Horodecki, P. Horodecki, M. Horodecki, K. Horodecki, Rev. Mod. Phys. **81**, 865 (2009)
11. K. Berrada, A. Chafik, H. Eleuch, Y. Hassouni, Quantum Inform. Process. **9**, 13 (2010)
12. M. Schlosshauer, Rev. Mod. Phys. **76**, 1267 (2004)
13. B. Bernardo, Braz. J. Phys. **44**, 202 (2014)
14. X.S. Ma, A.M. Wang, X.D. Yang, F. Xu, Eur. Phys. J. D **37**, 135 (2006)
15. K. Berrada, M. El Baz, H. Eleuch, Y. Hassouni, Int. J. Mod. Phys. C **21**, 291 (2010)
16. L.-M. Duan, G.-C. Guo, Phys. Rev. Lett. **79**, 1953 (1997)
17. D.A. Lidar, I.L. Chuang, K.B. Whaley, Phys. Rev. Lett. **81**, 2594 (1998)
18. S. Maniscalco, F. Francica, R.L. Zaffino, N. Lo Gullo, F. Plastina, Phys. Rev. Lett. **100**, 090503 (2008)
19. P.K. Jha, H. Eleuch, Y.V. Rostovtsev, Phys. Rev. A **82**, 045805 (2010)
20. H. Eleuch, S. Guerin, H.R. Jauslin, Phys. Rev. A **85**, 013830 (2012)
21. A. Imamoglu, D.D. Awschalom, G. Burkard, D.P. DiVincenzo, D. Loss, M. Sherwin, A. Small, Phys. Rev. Lett. **83**, 4204 (1999)
22. S.B. Zheng, G.C. Guo, Phys. Rev. Lett. **85**, 2392 (2000)
23. H. Eleuch, R. Bennaceur, J. Opt. A **5**, 528 (2003)
24. H. Jabri, H. Eleuch, T. Djerad, Laser Phys. Lett. **2**, 253 (2005)
25. C. Sames, H. Chibani, C. Hamsen, P.A. Altin, T. Wilk, G. Rempe, Phys. Rev. Lett. **112**, 043601 (2014)
26. C. Hermann-Avigliano, N. Cisternas, M. Brune, J.-M. Raimond, C. Saavedra, Phys. Rev. A **91**, 013815 (2015)
27. H. Eleuch, A. Prasad, Phys. Lett. A **376**, 1970 (2012)
28. Y.C. Liu, X. Luan, H.K. Li, Q. Gong, C.W. Wong, Y.F. Xiao, Phys. Rev. Lett. **112**, 013815 (2014)
29. E.A. Sete, H. Eleuch, Phys. Rev. A **82**, 043810 (2010)
30. F. Haas, J. Volz, R. Gehr, J. Reichel, J. Esteve, Science **344**, 180 (2014)
31. H. Eleuch, Int. J. Mod. Phys. B **24**, 5653 (2010)
32. A.K. Ekert, Phys. Rev. Lett. **67**, 661 (1991)

33. M. Abdel-Aty, M.J. Everitt, Eur. Phys. J. B **74**, 81 (2010)
34. M.L. Hu, Phys. Lett. A **375**, 922 (2011)
35. M.L. Hu, Ann. Phys. **327**, 2332 (2012)
36. C.H. Bennett, D.P. DiVincenzo, Nature **404**, 247 (2000)
37. Sh. Barzanjeh, H. Eleuch, Physica E **42**, 2091 (2010)
38. H.W. Lee, Phys. Rep. **259**, 147 (1995)
39. W.P. Schleich, *Quantum Optics in Phase Space* (Wiley-VCH, Berlin, 2001)
40. E. Wigner, Phys. Rev. **40**, 749 (1930)
41. K. Husimi, Proc. Phys. Math. Soc. Jpn **22**, 264 (1940)
42. R.J. Glauber, Phys. Rev. **131**, 2766 (1963)
43. Héctor Moya-Cessa, P.L. Knight, Phys. Rev. A **48**, 2479 (1993)
44. H.A. Hessian, A.-B.A. Mohamed, Laser Phys. **18**, 1217 (2008)
45. A.-B.A. Mohamed, Phys. Lett. A **374**, 4115 (2010)
46. A. Banerji, R.P. Singh, A. Bandyopadhyay, Opt. Commun. **330**, 85 (2014)
47. Hai-WoongLee, Opt. Commun. **337**, 62 (2015)
48. W. Leonski, S. Dyrting, R. Tanas, Laser Phys. **7**, 54 (1997)
49. A. Baas, J.Ph. Karr, H. Eleuch, E. Giacobino, Phys. Rev. A **69**, 23809 (2004)
50. H. Eleuch, J. Phys. B: At. Mol. Opt. Phys. **41**, 055502 (2008)
51. H. Eleuch, Appl. Math. Inform. Sci. **3**, 185 (2009)
52. W.H. Louisell, *Quantum Statistical Properties of Radiation* (Wiley, New York, 1973)
53. H. Eleuch, Eur. Phys. J. D **49**, 139 (2008)
54. H. Eleuch, N. Ben Nessib, R. Bennaceur, Eur. Phys. J. D **29**, 391 (2004)
55. H.J. Carmichael, *Statistical Methods in Quantum Optics* (Springer, Berlin, 2007), Vol. 2
56. H.J. Carmichael, R.J. Brecha, P.R. Rice, Opt. Commun. **82**, 73 (1991)
57. R. Horodecki, P. Horodecki, M. Horodecki, K. Horodecki, Rev. Mod. Phys **81**, 865 (2009)
58. W.K. Wootters, Quantum Inform. Comput. **1**, 27 (2001)
59. M.B. Plenio, V. Vedral, Contemp. Phys. **39**, 431 (1998)
60. V. Vedral, M.B. Plenio, M.A. Rippin, P.L. Knight, Phys. Rev. Lett. **78**, 2275 (1997)
61. M. Araki, E. H Lieb, Commun. Mat. Phys. **18**, 160 (1970)
62. M.A. Manko, V.I. Manko, Phys. Scr. T **160**, 014030 (2014)
63. K.E. Cahill, R.J. Glauber, Phys. Rev. **177**, 1882 (1968)
64. K.E. Cahill, R.J. Glauber, Phys. Rev. **177**, 1857 (1968)
65. P. Bertet, A. Auffeves, P. Maioli, S. Osnaghi, T. Meunier, M. Brune, J.M. Raimond, S. Haroche, Phys. Rev. Lett. **89**, 200420 (2002)
66. K. Laiho, K.N. Cassemiro, D. Gross, C. Silberhorn, Phys. Rev. Lett. **105**, 253603 (2010)
67. L. Ding, C. Baker, P. Senellart, A. Lemaitre, S. Ducci, G. Leo, I. Favero, Appl. Phys. Lett. **98**, 113108 (2011)
68. S. Anguiano, G. Rozas, A.E. Bruchhausen, A. Fainstein, B. Jusserand, P. Senellart, A. Lemaitre, Phys. Rev. B **90**, 045314 (2014)
69. A. Fainstein, N.D. Lanzillotti-Kimura, B. Jusserand, B. Perrin, Phys. Rev. Lett. **110**, 037403 (2013)